A. NUCLEAR FUELS

4. BASIC STUDIES

INTRODUCTION

Basic studies are sometimes needed for proper understanding of a particular phenomenon. Development of Master Sintering Curve (MSC) for AHWR fuel composition, which provided a new insight into the sintering phenomena and predicted the densification behaviour under a set of arbitrary time-temperature excursion, is a good example of this. Molecular dynamic simulation to predict thermophysical properties of UO_2 at temperatures much beyond the experimental capabilities or prediction of properties like elastic modulus, shear modulus, bulk modulus, fracture toughness etc. by ultrasonic velocity measurement are other examples of the usefulness of basic studies.

4.1 CLASSICAL MOLECULAR DYNAMICS SIMULATION OF UO_2

Thermo-physical and thermo-mechanical properties as well as transport phenomena of nuclear fuels are of special interest to the fuel designers for better understanding and prediction of in reactor fuel performance. Moreover during the loss of coolant accident (LOCA) condition when fuel melt down could occur; the engineering design parameters of the reactor components are of paramount importance. Such a situation also demands the relevant properties to be evaluated at or near melting point.

It is not always possible to determine experimentally various thermophysical and other properties at very high temperature or pressure since majority of the instruments have their own limitations. Hence, computer modeling provides a useful route to simulate such extreme conditions e.g. thermal conductivity of the fuel at LOCA condition. With the advent of modern powerful computers such simulation 'experiments' are gaining popularity.

In recent years a number of studies on Molecular Dynamics (MD) simulation of UO_2 have been published and it was observed that it is quite simple to simulate UO_2 system using classical pair potential in order to get various thermophysical and transport properties. The same could be done with the help of shell model. Non-equilibrium molecular dynamics (NEMD) could play a potential role to get various useful kinetic and transport properties of the system (e.g. thermal conductivity).

It has been seen that for some systems there does not exist any unique set of pair-potential parameters that are able to produce all the thermodynamic properties of that system at all temperature ranges and this is known as the transferability problem. The sustenance of this transferability problem of the pair-potential parameters for various oxides, silicates and some other compounds is still there and so also for the UO_2 system.

In this work emphasis has been given on the selection of the potential model, especially the fitting of the potential parameters and to study the lattice parameter variation, thermal expansion, mean square displacement of cation and anion and isothermal compressibility of UO_2 as a function of temperature with the help of these fitted potential parameters.

■ Potential Model

Bushing- Ida type of potential along with Morse type potential model is useful while simulating a semi-ionic system; where the long range Coulomb interactions, core repulsion and the Van dar Wall's weak attraction are considered. Along with that the Morse type potential is also applicable only for anion-cation pair.

■ Simulation Techniques

UO_2 holds stable fluorite structure (CaF_2 type) and each unit cell contains 4 U^{4+} ion and 8 O^{2-} ion. The MD cell was constructed with an array of 3X3X3 supercells in three mutually orthogonal directions totaling 108 cations and 216 anions. The size of MD cell was determined by the correctness of Ewald sum technique that was used to calculate the long range Coulombic interaction part.

The initial random velocity was chosen from the Maxwell-Boltzmann distribution at 298K. The equation of motion was integrated using Beeman's algorithm, which is of predictor-corrector type, with the unit time step of $2.0X10^{-15}$s. Only constant pressure-temperature (NPT) simulation was performed using Nosé -Hoover thermostat to control the temperature. Before accumulation of the thermodynamic data, an equilibrium run of $2X10^4$ time steps were made at desired temperature and pressure. During the simulation Parrinello-Rahman constant stress method was applied in order to judge the structural reproducibility of the system along with the required pressure control. The calculation was performed by the popular molecular dynamics code MOLDY in LINUX platform using PC.

To ensure effective coupling between system and external pressure bath, the extended system mass parameter was approximated using ultrasonic velocity measurement in UO_2 at each temperature. It ensures better pressure control of the concerned system.

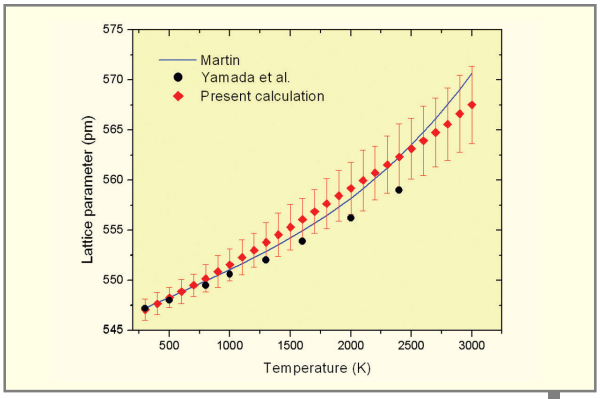

Lattice parameter of UO_2 as a function of temperature

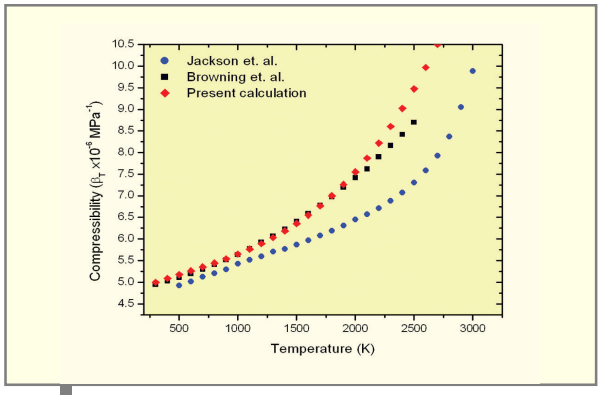

Isothermal compressibility of UO_2 as a function of temperature

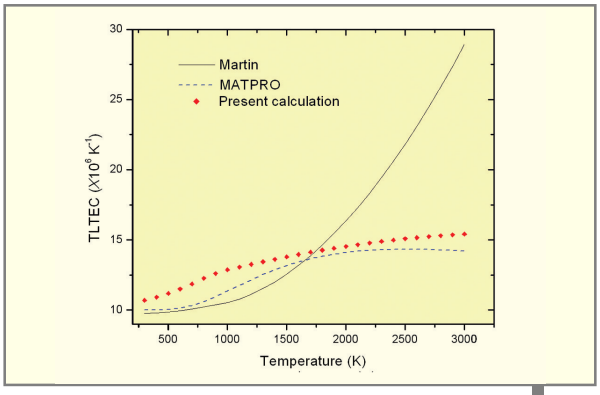

True linear thermal expansion coefficient of UO_2 as a function of temperature

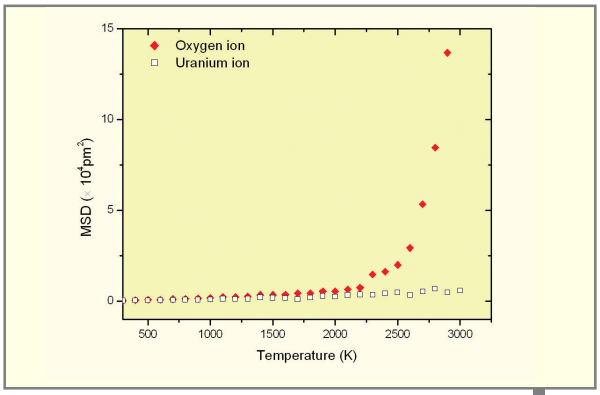

Mean square displacement of U and O ions in UO_2 lattice as a function of temperature : also note the Bredig transition temperature

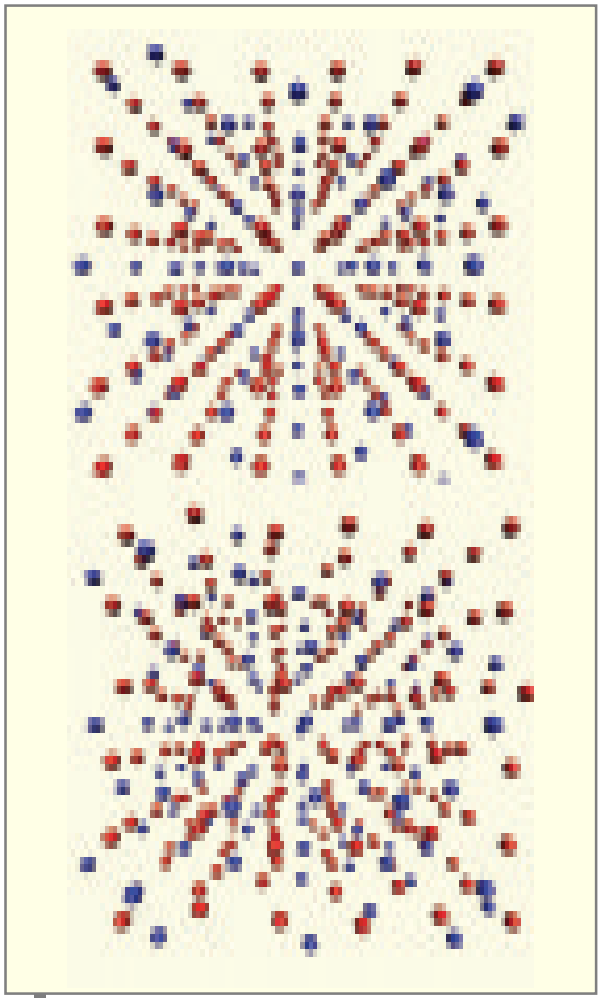

Ionic arrangements in UO_2 lattice; blue:U and red:O; at 300 and 1500K

4.2 COMPATIBILITY OF Pb-Bi ALLOY WITH GRAPHITE

High temperature nuclear reactors generally use gas as coolant, however, liquid metal or alloy could be a better alternative because of their higher thermal efficiency which can make the reactor more compact. Lead Bismuth Eutectic (LBE) alloy (Pb: 55.5 wt %, Bi: 44.5 wt %) could be a potential candidate material as coolant for the Compact High Temperature Reactor (CHTR) because of its several favourable properties like high thermal conductivity, high boiling point and low vapour pressure]. While high boiling point (1943 K) eliminates the possibility of over pressurization and prevents boiling and explosion due to over heating of the core, low melting point (397 K) reduces the chances of freezing of the alloy in the primary coolant circuit. It has low chemical activity, which makes it safe against possibility of fires and explosion in the event of coolant leakage. It also act as a shield for high energy 'γ' radiation in the reactor. Besides, LBE has a negative void coefficient of reactivity, which makes the reactor safe in case of loss of coolant accident (LOCA). Apart from these, low vapour pressure and low volume contraction on solidification also makes it attractive as a coolant. However, the compatibility of the coolant with the structural and fuel cladding materials should be explored for the deployment of lead based alloys as coolant for such reactors. Lead bismuth alloy buttons of eutectic composition (Pb: 55.5 wt.%, Bi: 44.5 wt%) were made in an arc furnace.

Pure graphite of density 1.78 gm/cm^3 was taken in the form of crucibles with threaded lid. The crucibles were dedusted and degassed by soaking at 573 K for 1 hr, following quenching in boiling water and then subsequent heat treatment at 573 K for 30 min. Small pieces of the LBE alloy were filled in the graphite crucibles and were encapsulated in quartz capsules under helium atmosphere.

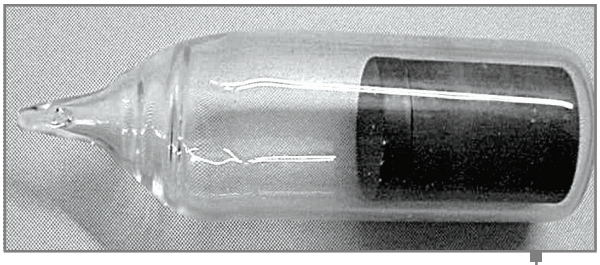

Graphite crucible containing Pb-Bi alloy encapsulated in quartz capsule

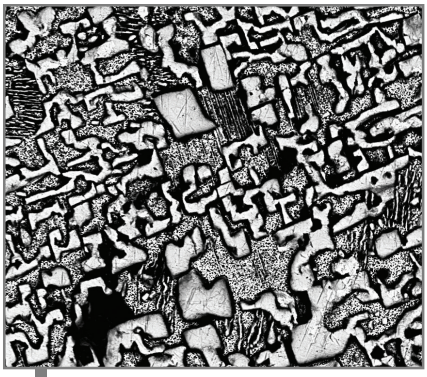

Scanning Electron Micrograph of Pb-Bi alloy of eutectic composition

The graphite crucibles containing the LBE alloy enclosed in quartz capsules were isothermally annealed at 1073 K, 1173 K, 1273 K and 1373 K for various time intervals ranging from 100 to 1000 hours in resistance heating furnace.

After heat treatment for the specified times and temperatures, the graphite crucibles were sectioned longitudinally using a slow speed diamond saw. The surface of the cross-sections was polished using standard metallographic techniques. The samples were characterized using an electron probe micro analyser (EPMA). The EPMA used was equipped with three wavelength dispersive spectrometers (WDS). Line scans of 'Pb', 'Bi', and 'C' and 'Y' were acquired across the interface to determine distribution of each of the elements.

Secondary electron image (SE) of the graphite/LBE interface of the crucible heat treated at 1073 K for 100 hrs indicates a layer of compound along the interface having uniform thickness throughout. The intensity profile of Pb(Lα), Bi(Lα) and C(Kα) X-ray lines were taken across the interface along a line AB and it indicates that the compound basically contains Pb and C. The compound was quantitatively analysed by fixing the beam on it and correcting the intensities of Pb and C. It was also found that the compound was PbC_2. Phase diagram of Pb-C also confirms the presence of PbC_2 in the system. It was also observed that the layer of PbC_2 formed at the interface adhered to the LBE alloy and a gap developed between the graphite and PbC_2 layer when the graphite crucible containing liquid LBE was cooled down to room temperature after the compatibility test. This is essentially due to the differences in coefficient of thermal expansions of LBE alloy, PbC_2 and graphite. Similar reactions

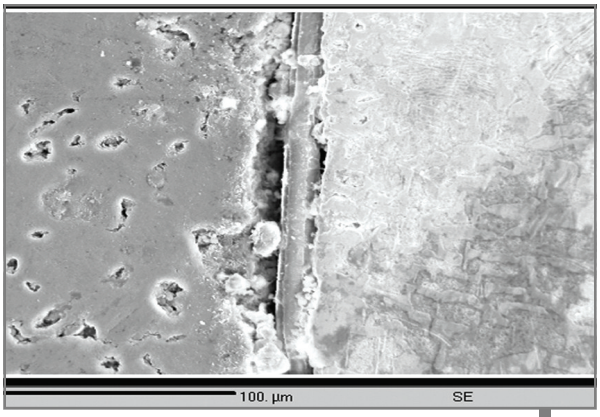

Scanning Electron Micrograph of the Interface of Pb-Bi eutectic alloy showing PbC_2 interface alloy

were also observed in other crucibles heat-treated at various temperatures and time intervals.

The data points were fitted with a straight line using the least square method and can be represented by the following relation,

$$w = 1.29x10^{-5} + 8.62x10^{-9}\sqrt{t}.$$

It was estimated that a zone of 61.3 µm wide would develop in 1 year and 121 µm in 5 years. Since the growth is parabolic in nature, initially the reaction layer forms very rapidly but the growth rate decreases after some time and becomes very slow subsequently. The growth of the reaction zone is thus diffusion controlled.

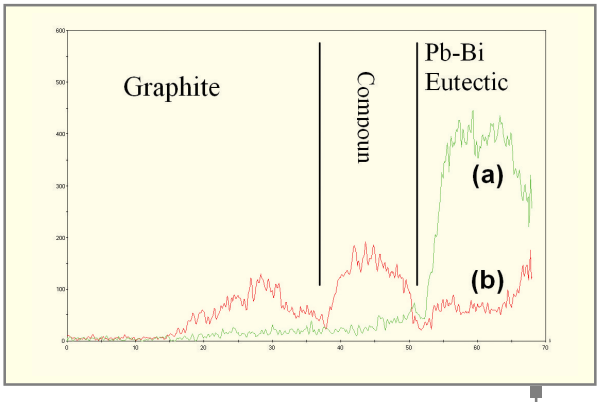

Intensity profile along the line perpendicular to Pb-Bi/graphite interface; (a) Pb(Lα) and (b) Bi(Lα)

4.3 DEVELOPMENT OF N-A FDM BASED CODE TO DETERMINE THE 3-D SIZE DISTRIBUTION OF HOMOGENEOUSLY DISPERSED SPHERICAL SECOND PHASE FROM MICROSTRUCTURE

In the field of powder metallurgy and composite material it is of great interest to know the actual 3-D distribution of porosity and/ or the second phase particles in the matrix. In case of ceramic nuclear fuel the size distribution of pores determines the in-reactor densification behaviour and swelling of the fuel pellet. A classical example is the nodular cast iron, where inoculant is used to allow the graphite particles to grow in spherical shape in ferrite matrix and the size distribution of such nodular graphite particles determines various bulk properties of the material; like elastic modulus, ductility etc.

The present endeavour is to determine the 3-D distribution from its 2-D counterpart by solving an integral equation analytically. However, in order to form an executable code, one needs to have a better insight of this formulation and its overall mathematical behaviour. In the present study, emphasis has been given on the behavioural features of the formulation considering various possible cases and checkpoints. Eventually the algorithm has been implemented for nodular cast iron along with proper experimental verification.

This formulation was based on the following basic assumptions:
i) All Particles are spherical in shape.
ii) Particles are distributed homogeneously in the matrix in non-overlapping manner with continuous size variation.
iii) Maximum diameter of the cross sectional circle (as seen in microstructure) is equal to the diameter of the largest particle.

The probability that a particle of diameter z will appear as a circle with a diameter between x and $x+dx$ on a horizontal sectional plane within a cube of unit length can be expressed as

$$p(x) = \frac{x}{\sqrt{z^2 - x^2}}dx \quad \forall x \le z \tag{1}$$

Since $N_a(x)$ is the sectional number density (i.e. 2-D distribution) in the diametric interval of $[x,x+dx]$ which resulted from the actual particle number density (i.e. 3-D distribution) N_v in the diametric range of $[x,\infty]$; so the relation between these two quantities can be expressed as –

$$N_a(x) = \int_x^\infty p(x) \cdot N_v(z)dz \tag{2}$$

$N_v(z)$ is unknown and $N_a(x)$ is the known quantity, hence Eqn. (2) can be regarded as Volterra equation of the second kind. Solution of this equation for an arbitrary diameter u is given by

$$N_v(u) = -\frac{2}{\pi}\cdot\frac{d}{du}\int_u^\infty \frac{N_a(x)}{\sqrt{x^2 - z^2}}\,dx \qquad (3)$$

Assuming that the groups are arranged in arithmetic progression with group width (or class interval) of Δ and D_m is the largest diameter observed in the microstructure and also the largest particle diameter (i.e. $D_m = k\Delta$) then applying finite difference method on Eqn. (3) and subsequent integration yields for the j^{th} group

$$N_v(j)\Delta = A(j,j)N_a(j) + \sum_{i=j+1}^{k} A(i,j)N_a(i) \qquad (4)$$

where,

$$A(j,j) = 1 \quad \text{for } (j=1)$$
$$= \frac{2}{\pi}\ln\left(\frac{j+\sqrt{j^2-(j-1)^2}}{j-1}\right) \quad \forall (j>1) \qquad (5a)$$

$$A(i,j) = \frac{2}{\pi}\ln\left(\frac{i+\sqrt{i^2-(j-1)^2}}{i+\sqrt{i^2-j^2}}\,\frac{i-1+\sqrt{(i-1)^2-j^2}}{i-1+\sqrt{(i-1)^2-(j-1)^2}}\right) \quad \forall (i>j) \qquad (5b)$$

Experimental Procedure

Nodular cast iron samples were obtained from Electrosteel Casting Ltd., Khardah Works, West Bengal, India. The specimens were cut from a fully annealed spun pipe (nominal diameter 250 mm). A typical optical micrograph is shown below.

After grinding and polishing the 2-D distribution was generated using Image Pro Plus (v 4.1) software. It may be noted that the 2-D distribution has to be scaled down with respect to the area of interest (AOI); because the formulation considers the AOI as a unit area. Scaling up the area instead of scaling down may give erroneous results because of small AOI and hence poor statistical sampling.

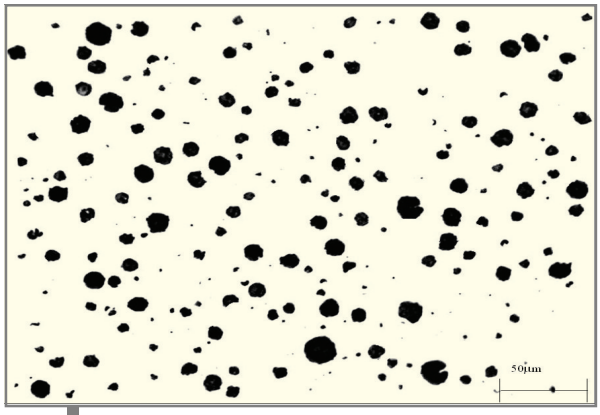

Typical photomicrograph of nodular cast iron, after grinding and polishing (contrast enhanced followed by intensity calibration)

Since the present formalism is based on a probabilistic approach a large number of sampling was needed. For the present study the 2-D distribution was made from 20 different places, comprising 5 different places across the thickness from each of the four different sections of the specimens and then merged all of them in order to get a representative 2-D distribution. The final 2-D distribution was fed into the code to generate the desired 3-D distribution of graphite nodule.

In order to validate the model the carbon balance method was used as follows

$$xD_{NCI} = 100\,pD_{Nd} + 0.007\,(1-p)D_{Fr}$$

where, x is wt. % of carbon in the sample and p is volume fraction of graphite nodule (obtainable from the model). D_{NCI}, D_{Nd} and D_{Fr} are the specific gravitiy of nodular cast iron, graphite nodule and ferrite respectively. The factor 0.007 denotes the wt % C present in the ferrite. The specific gravity of nodular cast iron (D_{NCI}) was measured and found to be 6.99. Specific gravity of ferrite (D_{Fr}) is taken same as a-iron i.e. 7.87 and the same for nodular graphite is 2.1. Carbon content in the sample was determined using the carbon analyzer where the known amount of milled pieces of the sample is heated under oxygen atmosphere upto 1773 K in an alumina crucible. CO present in the evolved gas is converted to CO_2 which is measured by infrared detector. After four analyses the mean value of carbon wt% was found to be 3.364.

Result and Discussions

The minimum detectable length being one pixel the spatial calibration gives the resolution of 0.45 μm at 200X. The maximum observed diameter was found to be 22.24 μm. The class interval (Δ) should be high enough to avoid excessive data discretisation and small enough to represent the meaningful classification of data. For the present study we took two values of Δ as 1.39 μm and 0.695 μm generating the number of classes as 16 and 32 respectively to build up two different 2-D distributions.

The sections with aspect ratio greater than 1 were converted to circular section with equal area of that section during the formation of the 2-D distribution. However it has been observed that the value of aspect ratio has never exceeded 1.76.

The total volume fraction of graphite nodule is derived using the following equation:

$$V_{total} = \frac{\pi \Delta^3}{12} \sum_{j=1}^{k} N_v(j).[(j-1)^3 + j^3]$$

It is interesting to note that the volume fraction histogram (shown below) shows a trend of a bell-shaped envelope curve that resembles the typical Gaussian type, though the diametric distribution (shown below) does not follow the Normal distribution. The wt% of carbon calculated from the volume

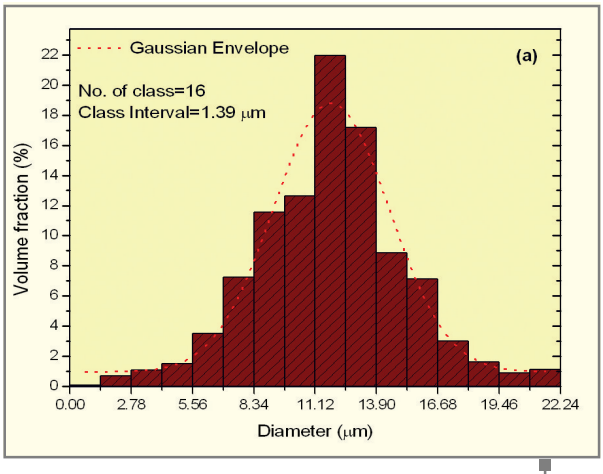

Histogram of volume fraction obtained from 3-D diametric distribution with number of class 16

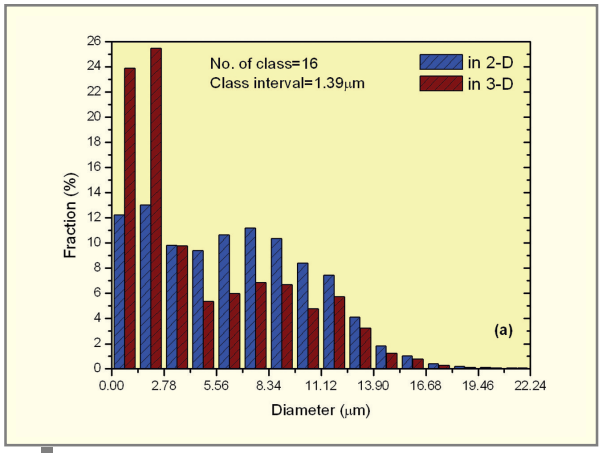

2-D and 3-D diametric distributions with number of class 16

fraction of individual class agrees reasonably well with that found from experiments. However, the small deviation of the calculated carbon content from the experimental value could be attributed to the following reasons. Firstly, the area conversion of the nearly circular shapes into the perfect circle will affect the 3- D distribution and hence the total carbon content. Another reason is the limitation in the resolution. Although higher resolution could give rise to better accuracy but number of screen shots required will increase sharply to cover the same AOI in lower resolution e.g. in 400X total 80 screen shots will cover the same AOI as for 20 screen shots in 200X.

Conclusions

A method is presented here to derive the diameter distribution of 3D homogeneously distributed spheres from measurements of the diameter distribution in random 2D sections through the distributed spheres. The solution of the analytical integral equation is very easy to implement in a computer code. It is possible to predict whether the particles are of uniform size or not. This model predicts the 3-D distribution more accurately than that of Saltykov's model. The future scope of this model is wide; porosity modeling and the effect of it in thermophysical properties can be determined for any material.

4.4 EFFECT OF TITANIA ADDITION ON HOT HARDNESS OF UO_2

Large-grained UO_2 fuel has been developed as a high burn-up fuel for LWRs. The large grain size increases the path length of the fission gas species for transportation to grain boundaries for coalescence and subsequent release. This helps in retention of the fission gases in the matrix without swelling. Though large grain size UO_2 pellet can be obtained by modifying powder characteristic and by increasing the sintering temperature and time, they are commercially not viable and are normally obtained by addition of dopants like Nb_2O_5, TiO_2, Cr_2O_3, and V_2O_5 etc., which also act as sintering aids. The grain size of UO_2 in the final sintered product, however, depends on the type and amount of dopants added.One of the prerequisites for addition of these dopants to the fuel is that they should not impair any other properties of the fuel. Literature reveals the effect of Nb_2O_5, TiO_2, Cr_2O_3 and V_2O_5 on the sintering behaviour of UO_2 and their effects on other properties. It has been reported that titania addition increases both grain sizes and thermal conductivity of UO_2 by about 10-15%. However, its effect on other material properties, particularly hot hardness has not yet been ascertained. In the present investigation attempts have been made to study the effect of TiO_2 on the hot hardness of sintered UO_2 fuel. This has been achieved by hardness measurements of UO_2 pellets from ambient to 1573 K in vacuum for titania content varying from 0.01w/o TiO_2 to 0.15w/o which resulted in grain size variation from 9.5 μm for UO_2 with 0.01 w/o to 94 μm for UO_2 with 0.15 w/o TiO_2. The grain size of the pure UO_2 pellet (control pellet) was of 9 μm under the same sintering condition.

■ Results and discussions

Photomicrographs of UO_2 containing different TiO_2 content (0.01- 0.15 w/o) are shown below. The photomicrographs indicate presence of equiaxed grains increasing in size with TiO_2 content with intragranular spherical pores of different sizes. No precipitates of UO_2-TiO_2 eutectic for UO_2 containing 0.15% TiO_2 could however be revealed by optical microscopy at grain boundaries (solubility limit TiO_2 at 1923 K in H_2 atmosphere is 0.13 w/o). The plot of hardness vs inverse square root of grain size at three different temperature ranges and the plot of hardness vs temperature for different grain sizes are shown

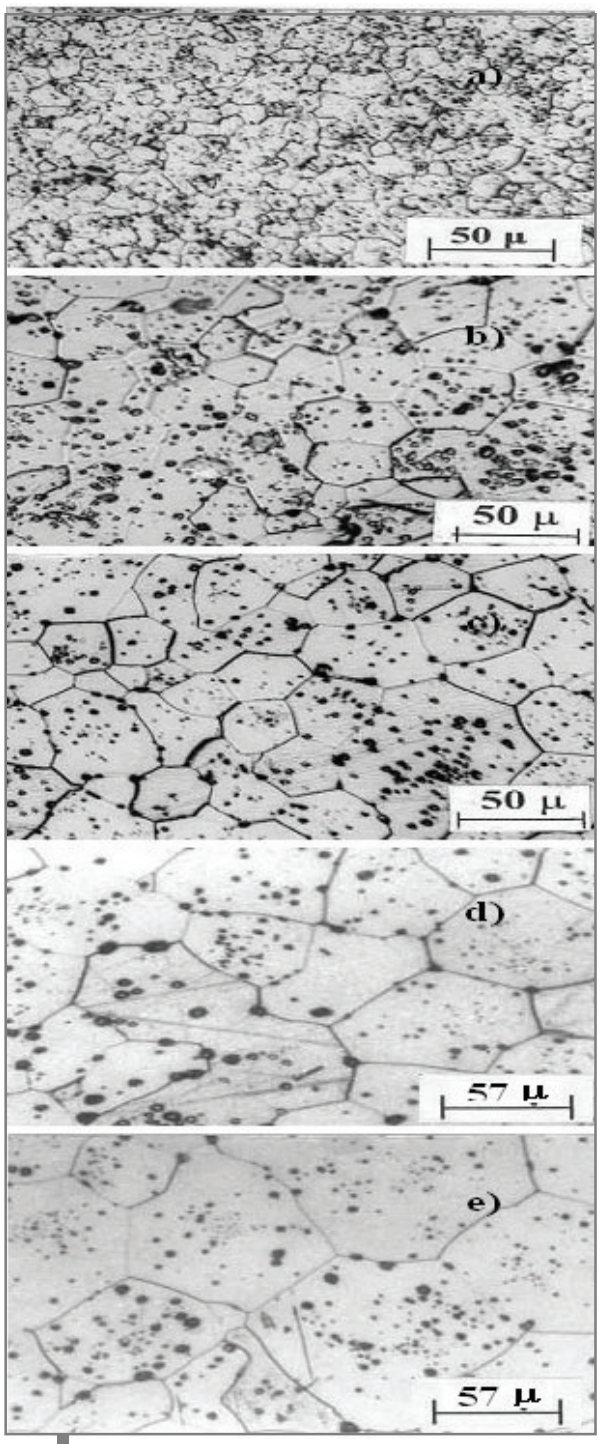

Photomicrographs of sintered UO_2 pellets with different TiO_2 content; [% TiO_2, Grain size]
a) (0.01%, 9.5μm; b) (0.05%, 18μm
c) (0.10%, 60μm d) (0.13%, 80μm
e) (0.15%, 94μm)

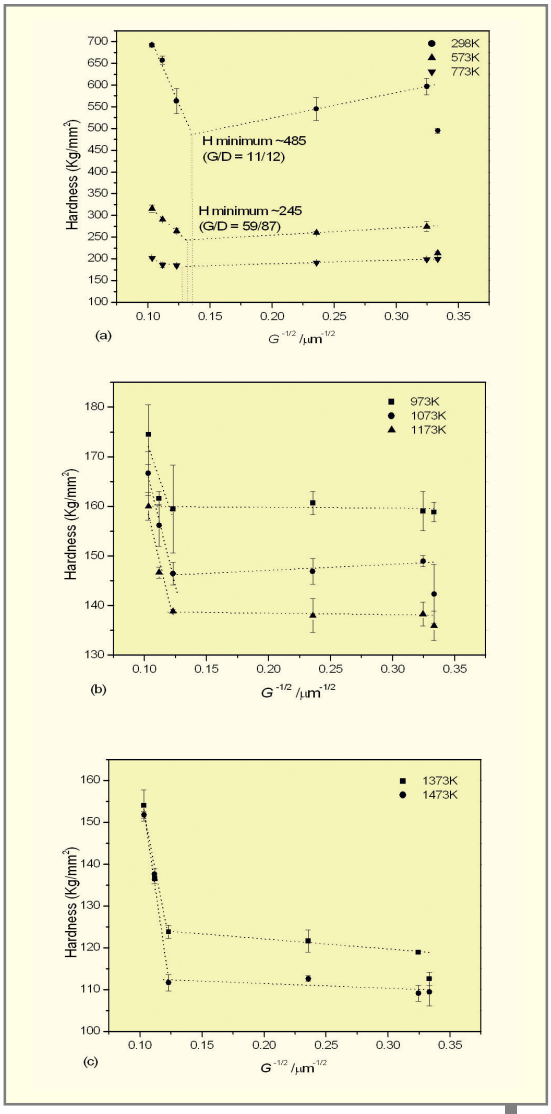

Variation in hardness as a function of $1/\sqrt{G}$ at three different temperature zones : fitted lines are indicated by dotted line

in figure. It should be noted that grain size as well as TiO_2 content influence hardness value at any temperature and also they are interrelated. However, the results have been discussed into three categories signifying the effect of TiO_2 content, grain size and temperature.

The effect of TiO_2 content, grain size and temperature on hardness and their complex interrelationship could be explained as follows:

Hardness of UO_2 increases with increase in TiO_2 content at any temperature and hence, the fuel becomes less and less plastic although grain size increases many folds e.g. 9μ to 94μ. This increase in hardness could be attributed to solid solution hardening by increasing amount of

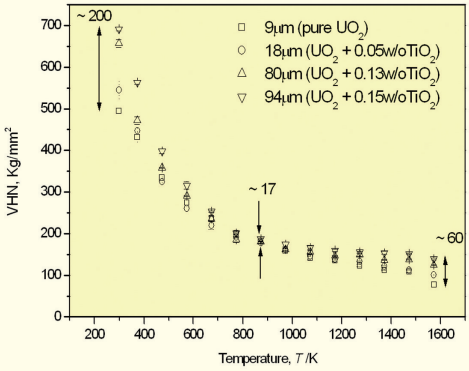

Variation in hardness with temperature. dH/dT for high grain size is sharp than that for low grain size in low temperature zone. But at higher temperature it is reversed

lattice strain induced by more and more TiO_2 addition within the solubility range. The hardening effect could also be attributed to the hindrance of the dislocation motion by pinning due to the presence of TiO_2 solute atom in UO_2 or precipitates (at high TiO_2 content, low temperature condition).

It is very difficult to separate the effect of grain size and TiO_2 content on hardness since the grain size and TiO_2 content are interrelated. However, in order to ascertain the dependence of hardness (H) variation with grain size (G) at various temperatures (T), hardness was plotted as a function of inverse square root of G (based on Hall- Petch relationship). The plot of H vs. $G^{-1/2}$ shows the same trend like most of the oxide and non-oxide ceramic materials at room temperature i.e. with increasing grain size hardness first decreases, reaches a minimum and then increases. However, the same trend was not observed at higher temperature and in the present study the whole temperature range was divided into three regions, namely lower temperature ($T \leq 773K$), intermediate temperature ($773K < T \leq 1273K$) and high temperature ($T > 1273K$) region to discuss their effects on hardness.

At lower temperatures (T= 773K) hardness decreases sharply with decrease in grain size because of two reasons. Firstly, the diagonal length of indentation becomes comparable to that of grain size (i.e. G/D ratio ≈1) causing grain boundary spalling due to intergranular crack generation. This results in decrease in hardness. The tendency of spalling is often enhanced by the presence of porosity on grain boundary. Secondly, the lower grain size contains lower amount of TiO_2, which in turn reduces the hardness. These two factors together oppose the strengthening effect due to grain fineness (following Hall-Petch relation) and becomep- redominant. Further decease in grain size increases the hardness due to the effect of grain fineness over spalling. Hence a minimum H value is observed due to transition from grain boundary spalling domination to grain fineness domination. It has been observed that in the lower temperature range there is increase in hardness for the sample with grain size of 9.5 μm (UO_2+0.01w/oTiO_2) than that for 9 μm (pure UO_2), which is due to the addition of TiO_2 alone; since the grain size effect is negligible. Hence hardness data corresponding to 9 μm grain size has not been considered for the fit.

At intermediate temperature range (773K< T ≤ 1273K) the higher grain size shows similar trend in hardness (as observed at lower temperatures) with the exception that the slope is less due to less grain boundary spalling. However, at lower grain size, hardness does not increase as sharply as in case of lower temperature range. With decreasing grain size, on the contrary, it becomes almost independent of grain size. This could be attributed to lowering of grain boundary strength at this temperature range. Hence, the dislocation piled up stresses generated during indentation is released easily which, in turn, lowers the hardness. As the grain size dependency of hardness at lower grain size is not predominant at this temperature range, H minima is not much pronounced here.

In the higher temperature range (T > 1273K), higher grain size shows similar effect as mentioned above. However, with decrease in grain size, hardness gradually decreases. This is attributed to grain boundary sliding which becomes operative at high temperature. Accordingly, smaller the grain size, more weak it becomes, though, the decrease in hardness with respect to grain size is not much.

From the variation of hardness with temperature for different TiO_2 content, it is seen that the spread in hardness data is maximum at 298K (~ 200 VHN) and minimum at 873K (~17 VHN); whereas at 1573K it is ~60 VHN. The relation between hardness and temperature is given by the following equation:

$$H = A\exp(-BT)$$

where, H is Vicker's hardness, A is the extrapolated hardness value at 0 K (called intrinsic hardness) and B is the softening coefficient of the material. The values of A and B are dependent on the amount of additives or impurities, grain size etc. The slope of ln$H$ vs. T gives the softening coefficient (B). Since the deformation mechanism, as stated earlier, is different in the lower temperature range than that at higher temperature range; a distinct change in slope (i.e. $d(\ln H)/dT$ or B) is expected between lower and higher temperature regimes. The plot of ln$H$ vs. T for various TiO_2 content conform reasonably well to the exponential relationship between hardness and temperature. It is observed that the change in slope (i.e. $d(\ln H)/dT$) or the transition occurs between 600- 800K; depending upon the TiO_2 content. This transition refers to change in deformation mechanism. Below 700K, the rapid decrease in hardness with the increase of temperature could be attributed to the release of strain energy (due to titanium ion and other interstitials) by lattice dilation. Beyond 700K the rate of decrease in hardness is less due to the pinning of dislocations by the interstitials and fine precipitates of eutectic phase; such mechanism ensures that the variation in hardness is insensitive to temperature at least up to $0.6T_m$; resulting in lower value of $d(\ln H)/dT$ at high temperature regime. As TiO_2 content goes up the misfit strain increases which gives rise to higher intrinsic hardness value whereas with the lattice dilation (i.e. increasing T) more strain energy is released that caused higher value of softening coefficients as TiO_2 content increases.

4.5 DEVELOPMENT OF MASTER SINTERING CURVE AND SINTERING KINETICS STUDIES ON (Th-U)O_2 MOX PELLETS

The sintering parameters of many ceramic products are still decided by the ancient method of trial and error basis. The theory of Master Sintering Curve (MSC) provides a new insight into the sintering phenomena. MSC enables the prediction of the densification behaviour under arbitrary time-temperature excursions with the help of a minimum number of preliminary experiments. The procedure for development of a master sintering curve for AHWR fuel of composition ThO_2-3%UO_2 is described below:

■ Theory of Master Sintering Curve

The master sintering curve is derived from the densification rate equation of the combined-stage sintering model. The parameters in the sintering rate equations can be separated into two parts: (a) those related to the microstructure and (b) those related to time and temperature terms. These parts, which are on the opposite sides of the equation, are then related to each other experimentally. The temperature -dependent side of the equation can be represented by

$$\theta = \int (1/T) \exp(-Q/RT)dt \qquad (1)$$

where Q is the sintering activation energy, R is the gas constant, t is the instantaneous time and T the absolute temperature. The relationship between density ρ and θ is defined as the master sintering curve. For the construction of MSC, the integral of equation (1) and density should be known.

■ Activation energy of sintering

For construction of Master sintering curves (ρ versus θ), correct value of activation energy is required which can be available from literature or can be estimated with good precision from ρ versus θ data. To estimate the activation energy for sintering, firstly, a particular value of activation energy is chosen and ρ versus θ curves are constructed for each heating rate. If the curves fail to converge, a new value of activation energy is chosen and the calculations are repeated. This procedure continues until all the curves converge and the corresponding activation energy is the true activation energy for sintering. If the correct value of Q is chosen, all of the data converges to a single curve. The best estimate of Q will be the value of the minimum in the plot of mean residual squares versus activation energy.

■ Experimental

The green pellets of ThO_2-3% UO_2 for this study were prepared by the conventional powder metallurgy route. The procedure adopted for the fabrication of ThO_2-3% UO_2 green pellets are as follows:

a) milling of the as-received ThO_2 powder in a planetary ball mill
b) mixing/milling of the above milled ThO_2 powder with the required quantity of UO_2 powder for 4 h in a planetary ball mill with tungsten carbide balls
c) double precompaction of the above mentioned mixtures at 150 MPa
d) granulation of the precompacts
e) final cold compaction of the granulated powder at 300 MPa into green pellets of about 8 mm diameter and 7mm long.

To determine the shrinkage of (Th-U)O_2, a push rod type high temperature horizontal dilatometer was used. The dilatometric experiments were carried out using a flow rate of 18 l/h. The heating rate used for the above studies was 6, 12 and 20°C/min. For the determination of activation energy, the density data for ThO_2-UO_2 compacts obtained from the dilatometric data, and θ values obtained from the equation (1) are employed. A ρ-θ curve is then constructed for all the heating profiles for a chosen value of activation energy. The mean residual squares for the various values of activation energy have been calculated and the minimum has been found to be for 500 kJ/mol.

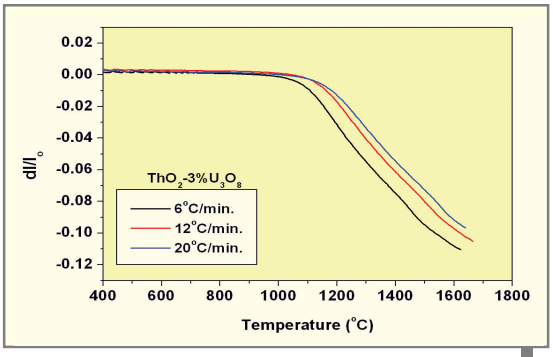

Shrinkage versus temperature plot for ThO_2-3%UO_2 in air for different heating rates

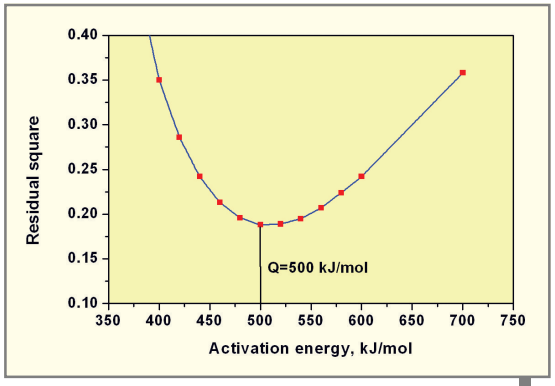

Mean residual squares for various values of activation energy

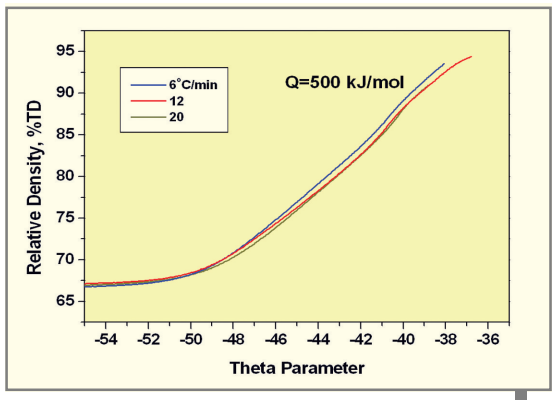

Master sintering curve for ThO_2-3%UO_2

From the knowledge of the activation energy, θ values are determined using (1) and are plotted against density (ρ). Such plot (master sintering curve) for ThO_2-3%UO_2 has been shown here.

Discussion

The following conclusions are drawn from the above study:

The concept of MSC can be used to calculate the activation energy for sintering. The activation energy for sintering for ThO_2-3%UO_2 was found to be 500 kJ/mol. The sinterability of powder compacts made from different powders and fabrication procedures under different thermal histories, can be characterized through the master sintering curve. The MSC curve can also be used as an aid to compare the sinterability of different powders and to know the effects of additives, atmosphere and fabrication procedure of sintering.

4.6 PHYSICAL PROPERTIES OF FUELS BY ULTRASONIC VELOCITY MEASUREMENT

Mechanical properties such as elastic modulus, hardness and yield stress of the fuel are very important for assessment of the Pellet Clad Mechanical Interaction (PCMI). The fracture properties of sintered fuel pellets for thermal reactors play an important role in the formation of stress-induced cracks and fission-gas swelling during reactor operation. Physical property like heat capacity of nuclear fuel is needed for reactor physics and safety calculations.

Some of the properties like Elastic modulus, Shear modulus, Bulk modulus and Poisson's ratio, compressibility, yield stress, yield strain, fracture toughness, fracture surface energy, Debye temperature, heat capacity, Gruneisen parameter and lattice vibrational frequency have been determined /calculated by ultrasonic velocity measurement method. The data generated for ThO_2+2%UO_2 and SIMFUEL based on UO_2 are highlighted.

Elastic constants like Elastic modulus, Shear modules, Bulk modulus and Poisson's ratio were determined from the measured longitudinal and shear wave velocities and density of the sample. Subsequently, using the elastic constants and measured micro hardness data yield stress was calculated. Yield strain was determined from yield stress and measured elastic modules. Fracture toughness was obtained using measured elastic constant and crack length generated at the corner of the indentations. Fracture surface energy and fracture modules were obtained from calculated fracture toughness. Debye temperature was calculated using ultrasonic longitudinal and shear wave velocities

and lattice parameter. Debye temperature was used to obtain harmonic contribution to specific heat of the materials. Gruneisen parameter which is an average measure of lattice anharmonicity, is calculated using specific heat. Subsequently lattice vibrational frequencies were calculated using Gruneisen parameter.

ThO_2 containing 2% UO_2 is the driver fuel for Advanced Heavy Water Reactor (AHWR). Sample pellets were prepared by conventional powder metallurgy route. It had a density of 96%TD.Simulated high burn-up nuclear fuels (SIMFUEL) attempts to replicate the chemical state and microstructure of the solid fission products generated in irradiated fuel so that detailed experiments can be undertaken without intense radiation fields to estimate the extent of degradation in the thermo-physical and mechanical properties of the fuel due to the presence of several fission products. Simulated UO_2 fuel (SIMFUEL) was prepared by adding high purity oxides of 11 different major fission products (Zr, Mo, Ce, Nd, Ru, Ba, La, Pd, Sr, Y and Rh) in UO_2 for an average burn up of 7000 MWd/ton for Indian PHWRs following ORIGEN code. UO_2 and SIMFUEL had densities of 95.72% T.D. and 90 % T.D. respectively.

Some of the properties of ThO_2+2% UO_2 and SIMFUEL based on UO_2 are given in the following tables and the stress /strain diagrams are shown in figures.

Property	UO_2	SIMFUEL
Shear modulus, G (Gpa)	76.3	70.25
Elastic modulus, E (Gpa)	201.10	181.64
Bulk modulus, K (Gpa)	185.07	147.94
Poison's ratio, γ	0.318	0.294

Heat capacity: C_p at constant pressure can be evaluated from the following relationship,

$$C_p = C_h + C_d + C_{el} + C_{anh} + C_{sch} + C_{SP} + \ldots\ldots$$

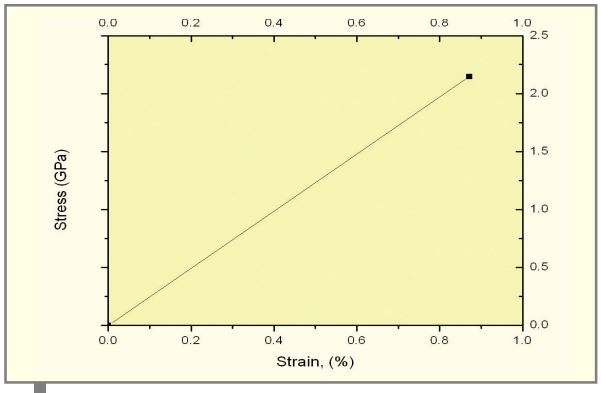

Stress-strain diagram of ThO_2+2%UO_2

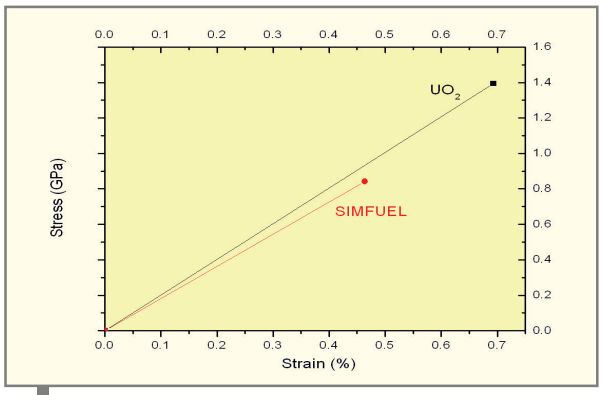

Stress-Strain diagram of UO_2 and SIMFUEL

where different contributions are: C_h is the harmonic due to lattice vibration, C_d is the dilational, C_{el} is the electronic, C_{anh} is the anharmonic, C_{sch} is the Schottky and C_{SP} for the formation of the small polaron to specific heat.

Debye temperature, which is determined by using measured longitudinal and shear wave sound velocities, was used in calculating harmonic contribution to specific heat of the ThO_2+2% UO_2, UO_2 and simulated UO_2 fuel. Other components of the specific heat which are contributing to total specific heat like dilational, anharmonic, schottky and small polaron were calculated from measured bulk modulus and other parameters obtained from literature. Specific heat of UO_2 and SIMFUEL were obtained from the summation of their individual contributions.

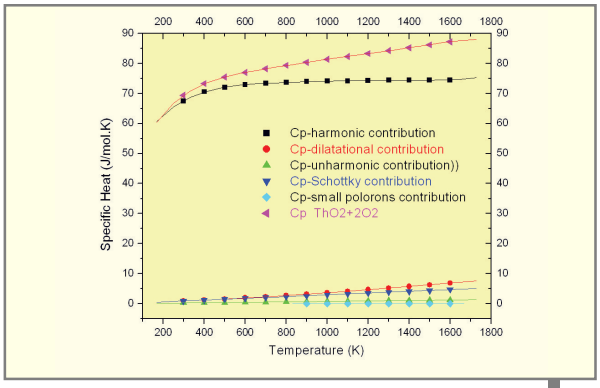

Graphical representation of contribution of each term to Specific heat of ThO_2+2%UO_2

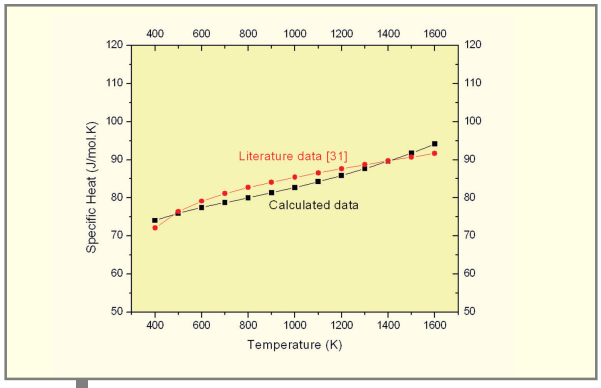

Specific heat of UO_2

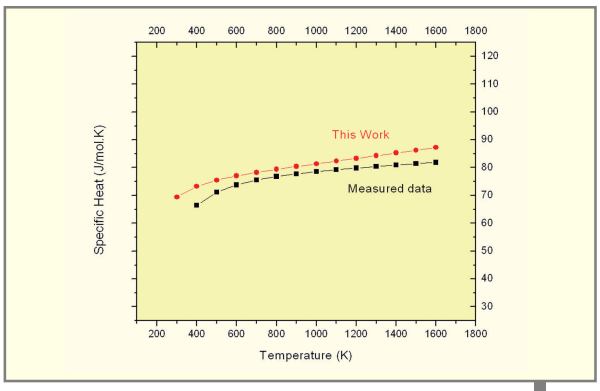

Specific heat of ThO_2+ 2% UO_2

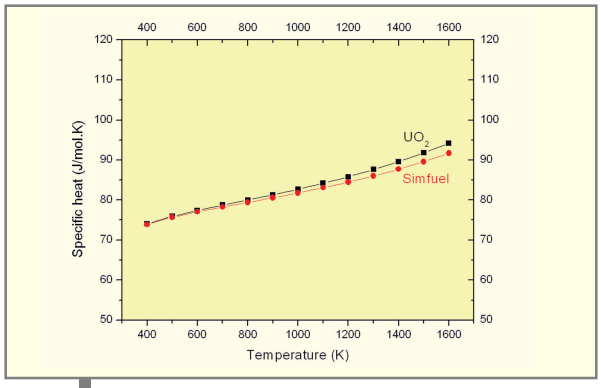

Specific heat of UO_2 and Simfuel

Sr no	Property	Numerical value at 298 K
1	Shear modulus, G GPa	97.899
2	Elastic modulus, E GPa	246.375
3	Bulk modulus, K GPa	169.9
4	Poison's ratio, γ	0.258
5	Compressibility, β Gpa^{-1}	5.898×10^{-3}
6	Micro-hardness (VHN)	787.11
	(Gpa)	7.72
7	Yield stress (Gpa)	2.147
8	Yield strain	0.0087155
	(%)	0.87145
9	Fracture Toughness, K_{1C} ($Mpa*m^{0.5}$)	1.203579
10	Fracture surface energy, J_{IC} (J/M^2)	2.7436
11	Fracture Modulus, E_f ($*10^{12}$) (Nm^{-2})	0.528
12	Debye Temperature, Θ_D, K	432.569
13	Specific heat, C_p (J/mol.K)	67.99
14	Gruneisen parameter	1.88

Physical and mechanical properties of ThO_2 – 2% UO_2 fuel